Acta Astronautica 201 (2022) 1–11

Contents lists available at ScienceDirect

Acta Astronautica

journal homepage: www.elsevier.com/locate/actaastro

Ultrasonic augers for improved transport of granular materials

Xuan Li [a], Xiaoniu Li [b], Tianlu Huang [b], Andrew Feeney [a], Kevin Worrall [a], Patrick Harkness [a,*]

[a] Centre for Medical and Industrial Ultrasonics, James Watt School of Engineering, University of Glasgow, Glasgow, G12 8QQ, UK
[b] State Key Lab of Mechanics and Control of Mechanical Structures, Nanjing University of Aeronautics and Astronautics, Nanjing, 210016, China

ARTICLE INFO

Keywords:
Ultrasonically assisted auger
Torque
Granular material
Helix angle

ABSTRACT

This paper explores the superposition of ultrasonic vibration on vertical rotating augers in a variety of granular media. Ultrasonic vibration is known to facilitate direct penetration of granular media, and it is anticipated that any related reduction in the torque requirements of a rotating system might improve augering performance. Experimental results suggest that, compared to the non-ultrasonic scenario, ultrasonically assisted augering significantly promotes the flow of granular media, while moderately reducing the torque required to operate the device. Furthermore, it was discovered that particle size, helix angle, and auger speed all affect the performance of the auger in different ways as the ultrasonic amplitude is adjusted.

1. Introduction

Ultrasonic vibration as a penetration aid with respect to granular materials was explored in some detail in 2017 [1], when it was demonstrated that the forces required to access the near subsurface could be substantially reduced. The proximate application was considered to be planetary exploration, where reduced forces could make it easier for penetrating probes to explore the dusty regolith of planets, moons, and asteroids.

However, it may be necessary to explore beneath rocky terrain as well, which requires drill systems to break the harder material. In every drill used in space to date, the rock breaking function has been combined with an auger to elevate the spoil out of the hole. This paper will explore whether sonication could similarly enhance the flow of spoil up such an auger, and therefore contribute to exploration of these more challenging terrains by reducing the effort required to rotate the drillstring. This would be particularly applicable for drillstrings less than a few wavelengths long.

Such an outcome may be possible because, in augering, the relatively low friction of the flights causes the spoil to preferentially slide up the scroll, rather than rotate at considerable speed against the higher frictional forces created at the borehole edge or auger tube wall [2]. If the reduced forces seen in sonicated penetration events could be recreated in a sonicated rotating system, then the differential friction effect that leads to elevation should be augmented and the auger should operate more effectively. This experimental study confirms that such an effect exists.

2. Material and methods

2.1. Granular material

The spoil created during actual drilling may have a wide range of properties, so for the purposes of this experiment a highly-repeatable substitute is used. Three batches of glass beads, with approximate diameters of 0.1 mm, 0.4 mm and 0.7 mm, are used, as per Fig. 1.

2.2. Ultrasonic augers

Fig. 2 shows the structure of the ultrasonic augers, as part of a Bolted Langevin Transducer (BLT) architecture. This configuration is comprised of a half-wavelength ultrasonic transducer (L500, Sonic Systems Ltd, Puckington, Ilminster, UK) tuned to resonate in its first longitudinal mode (L1) at around 20 kHz. Three cylindrical augers (made from Ti–6Al–4V material), with helix angles of 5°, 10° and 20°, were designed using the finite element analysis (FEA) software package Abaqus-Simulia (Dassault Systèmes, Vélizy-Villacoublay, France), manufactured, tuned to the full-wavelength, and then interfaced so that they can be attached to the transducer by means of a threaded stud. This forms a one-and-a-half wavelength device, resonating at around 20 kHz overall. The diameter of the cylindrical core of the auger is 34 mm, matching the transducer, and the outer diameter (across the auger scrolls) is 38 mm.

* Corresponding author.
E-mail address: Patrick.Harkness@glasgow.ac.uk (P. Harkness).

https://doi.org/10.1016/j.actaastro.2022.07.054
Received 22 June 2022; Received in revised form 18 July 2022; Accepted 30 July 2022
Available online 24 August 2022

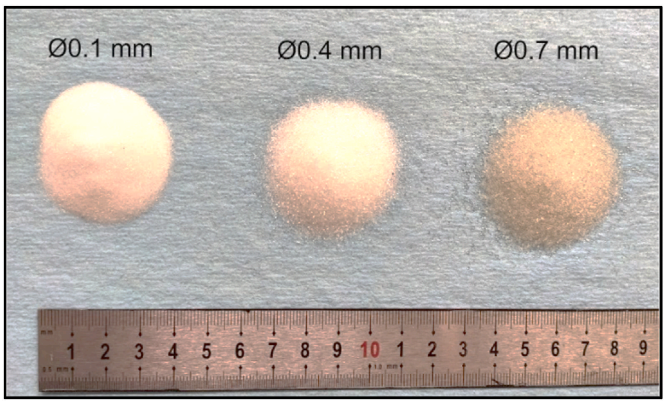

Fig. 1. Three different diameters of glass beads, used as granular materials for experimental purposes.

2.3. Characterisation

Characterisation of the ultrasonic augers is required to ensure that they operate as designed. The characterisation consists of an analysis of the electrical impedance and an experimental modal analysis.

(i) Electrical impedance analysis

Impedance analysis (IA) measurements were performed on all ultrasonic augers using a commercial device (4294 A, Agilent Technologies, Santa Clara, CA, USA). A swept signal of 1 V peak-to-peak over a bandwidth covering the frequency range of interest was applied, and the impedance spectrum was measured. The effective electromechanical coupling coefficient, k_{eff}, was calculated from the impedance spectrum data using equation (1) [3], providing an understanding of the ultrasonic augers' conversion efficiency from electrical energy to mechanical vibrations.

$$k_{eff}^2 = \frac{f_a^2 - f_r^2}{f_a^2} \quad (1)$$

f_a represents the anti-resonant frequency and f_r stands for the resonant frequency.

Mechanical Q factor, which is a measure of system damping derived from the peak response and the relative position of the half-power points, was also calculated from the impedance measurements to better define the bandwidth of the operating mode. The result was found to be consistent with the electromechanical findings, as described below.

(ii) Experimental modal analysis

Experimental modal analysis (EMA) was performed to understand the consistency of the vibrational mode shapes with the theoretical design. Frequency response functions (FRFs) were taken across a grid of vibration response measurement points, from which the modal parameters (frequency, damping, and mode shape) were extracted [4].

To generate the FRFs, a white noise excitation of 10 V_{rms} was generated by a signal generator (Quattro, Data Physics, Santa Clara, CA, USA) and amplified (RMX 4050HD, QSC Audio Products, Costa Mesa, CA, USA), before being supplied to the ultrasonic augers. A 3-D laser Doppler vibrometer (CLV3000, Polytec, Waldbronn, Germany) was used to measure three orthogonal components of the vibrational velocities from the grid points. Data acquisition and processing software (SignalCalc, Data Physics, Santa Clara, CA, USA) was then used to apply curve-fitting routines to extract the magnitude and phase data. Finally, the measured FRFs were exported to modal analysis software (ME'scopeVES, Vibrant Technology Inc, Centennial, CO, USA) to extract the

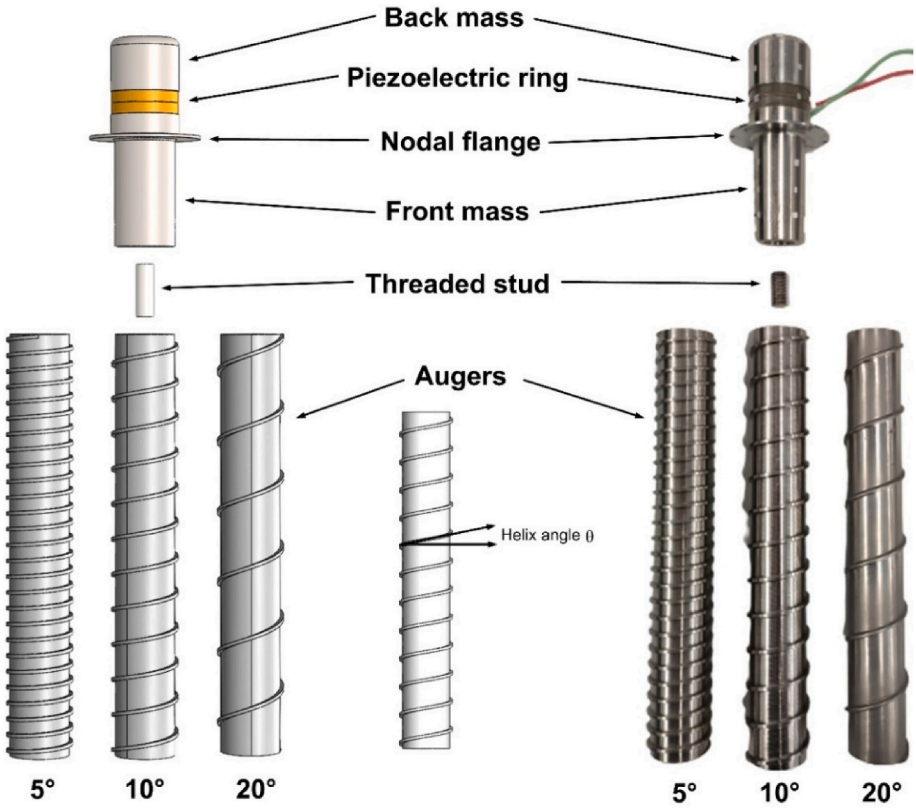

Fig. 2. Three ultrasonic auger models, nomenclatures, and the final devices. The augers are around 250 mm long, and the dimensions of the full stacks will be shown in Fig. 5.

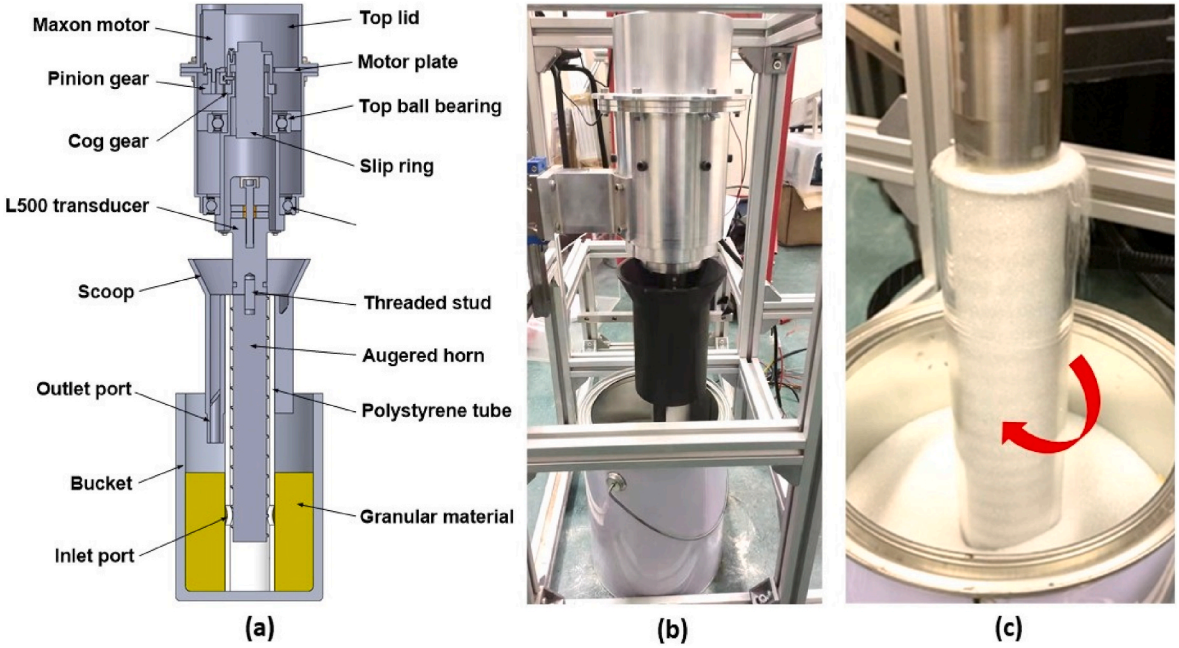

Fig. 3. (a) Cross-sectional view of the experimental platform of ultrasonic augers, (b) real experimental setup, (c) ultrasonically assisted auger in operation, with the granular media overtopping the tube (the scoop is not present).

modal parameters.

3. Experimental platform

The experimental platform is presented in Fig. 3 (a). Fig. 3 (b) and **(c)** illustrate the platform while the auger system is in operation. The red arrow indicates the direction of the rotation of the auger, inside the auger tube.

The ultrasonic stack is fixed to a spun housing through its nodal flange, with two contact bearings supporting the assembly. A cog gear is seated on the upper shoulder of the transducer housing, where it can be driven by a small pinion and a gearmotor (Maxon Group, Sachsein, Switzerland). To supply power to the spun assembly, a slip ring (MFS028-P0210-440V, Moflon Technology, Shenzhen, China) is used. A benchtop power supply (BK9129B, BK Precision, Yorba Linda, CA, USA) provides this power, with the power consumption of the gearmotor being recorded using an associated kit (IT-E132B) and LabView.

A bucket with granular media (shown in Fig. 1) is deployed directly underneath the ultrasonic auger. A transparent polystyrene tube is placed concentrically around the auger and is inserted in the granular material, to the very bottom of the bucket, to help stabilise the auger against oscillation and whirl. The tube has an inner diameter of 40 mm, leaving a 1 mm circumferential gap, and it has two 20 mm holes at the sides which act as inlet ports. A scoop made from polylactic acid is press fitted to the top of the tube, with an inclined surface that causes any material lifted by the auger to be directed towards an outlet port where it may be collected for transfer to a digital scale. In this way, the mass uplifted by the auger during an experiment may be recorded.

To energise the ultrasonic augers, a P100 control unit (Sonic Systems Ltd, Puckington, Ilminster, UK) is used. This vibration control unit employs a resonant frequency tracking technique [5], which automatically adjusts the output frequency to precisely match the resonance of the augers. A negative feedback control loop is integrated in the P100 control unit to maintain a constant displacement amplitude of the augers under load. The ultrasonic power consumption can be directly acquired from the P100 control unit.

4. Results

4.1. Electromechanical characteristics

To ensure the ultrasonic augers can be driven by the P100 control

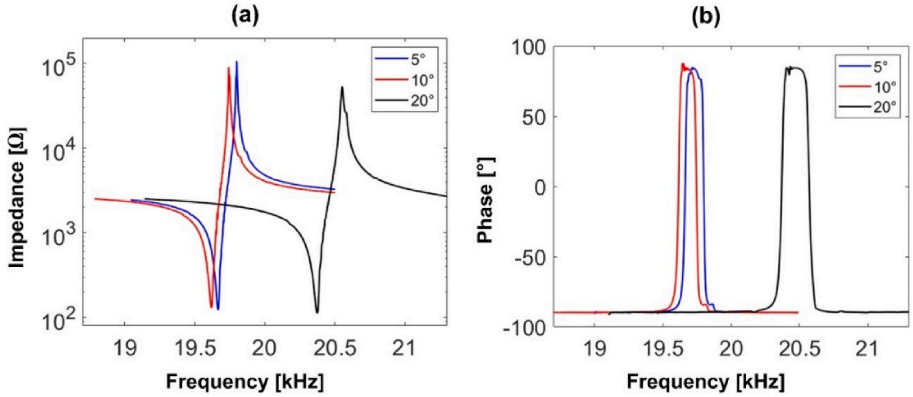

Fig. 4. Measured electrical impedance and phase of three different helix angle angers: (a) Impedance, (b) phase.

Table 1
Ultrasonic augers' electrical characteristics.

	5° auger	10° auger	20° auger
Resonance frequency f_r [Hz]	19,666	19,620	20,372
Anti-resonance frequency f_a [Hz]	19,799	19,745	20,552
Impedance magnitude Z [Ω]	123	130	112.4
Phase θ at f_r [°]	18.5	27	12.6
Coupling coefficient k_{eff} [−]	0.117	0.112	0.132
Q factor [−]	1093	998	886

unit under load (with the surrounding granular materials), the electromechanical characteristics will need to be confirmed.

The experimentally-measured impedance curves of all three helix angle augers are shown in Fig. 4, with the calculated electrical characteristics presented in Table 1. All three ultrasonic augers show resonance frequencies within the tracking range of 19.5–20.5 kHz, where the resonance can be maintained by the P100 control system. Also, the impedance magnitude values are all between 100 Ω and 150 Ω, close to the output impedance of the P100 control unit (50 Ω), to ensure maximum energy transfer. Electromechanical coupling coefficient values between 0.1 and 0.14 were found, suggesting a similar electromechanical energy conversion rate for all augers. Finally, Q factor values were found to be around 1000, demonstrating low losses in the systems as manufactured.

The simulated and experimentally identified vibration mode shape for the three ultrasonic augers at their one-and-half wavelength longitudinal modes are presented in Fig. 5, and the modal parameters have been summarised and presented in Table 2.

All three ultrasonic stacks present three nodes, located at the flange of the L500 transducer (allowing the ultrasonic stack to be clamped), and at roughly quarter-distance points from both ends of the actual augers. Amplification gain values (defined as the ratio of the displacement amplitude at the front face of the auger and end face of the back mass) are all consistently between 1.3 and 1.4. Resonance frequencies are all around 20 kHz for both simulation and experiment.

4.2. Final setup for the mass flow experiments

Three buckets of glass spheres with diameters of 0.1 mm, 0.4 mm, and 0.7 mm were prepared for the experiment (see Fig. 3 (b)). Displacement amplitudes at the base of the ultrasonic transducer were set to 0 μm (non-ultrasonic), 5 μm and 10 μm, amplified by a gain of 1.3–1.4 (see Table 2) to achieve a slightly higher amplitude at the tip of the augers. After a few exploratory runs, rotational speeds of 96 rpm, 144 rpm, and 192 rpm were selected for the 5° auger; 120 rpm, 180 rpm, and 240 rpm for the 10° auger; and 144 rpm, 216 rpm, and 288 rpm for the 20° auger. These speeds provided a broad range of throughput for each individual auger.

Each uplift cycle ran for 30 s and was repeated three times. Average output parameters of the systems, such as mass uplifted in grams, ultrasonic power consumption, motor power consumption and total power consumption were recorded. Finally, the torque exerted on the auger systems was calculated using equation (2), where T is the torque in Nm, P is power in Watts, and V is the rotational speed of the motor in rpm.

$$T = \frac{9548.8P}{V} \tag{2}$$

4.3. Mass flow

The mass of material uplifted over 30 s, for each auger system, is presented in Fig. 6. In general, when operating at a higher ultrasonic amplitude, more granular material was transported.

As expected, the steeper augers required faster rotation. It was also more challenging to sustain uplift in finer materials, so that in the

Table 2
Ultrasonic augers' mechanical characteristics.

	5° auger	10° auger	20° auger
Resonance frequency FEA f_r [Hz]	19,563	19,705	19,878
Resonance frequency EMA f_r [Hz]	19,668	19,584	20,340
Amplification gain FEA [−]	1.29	1.30	1.30
Amplification gain EMA [−]	1.41	1.35	1.32

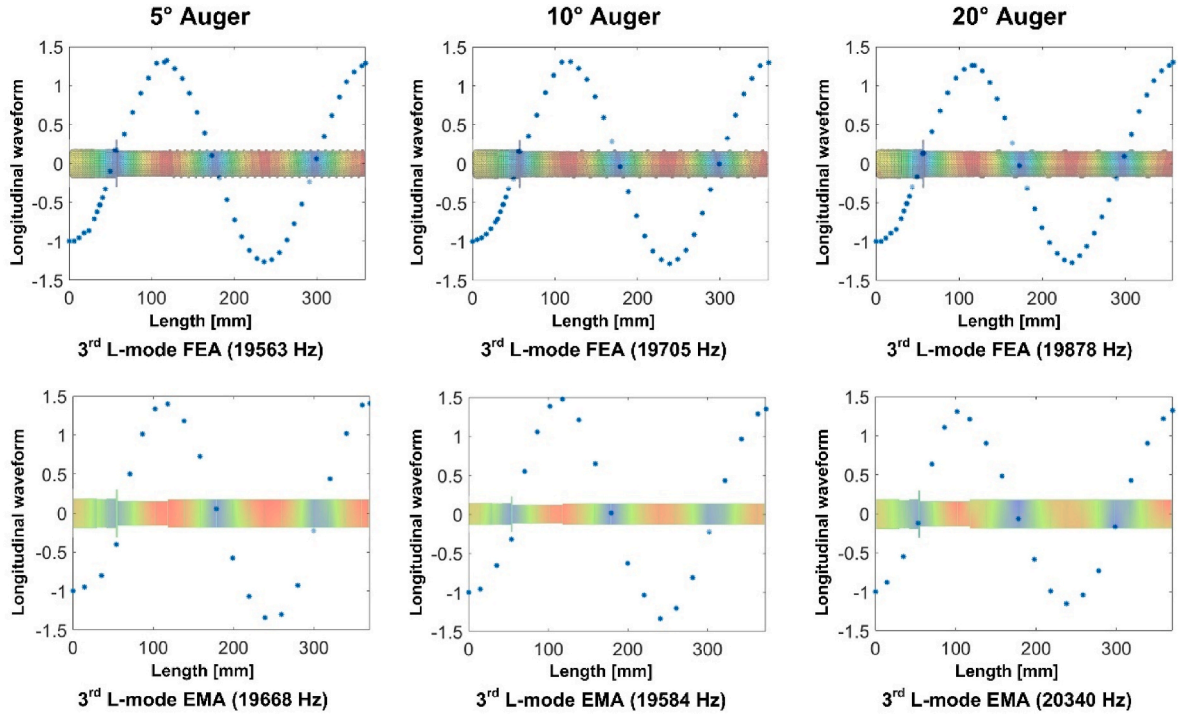

Fig. 5. Simulated and measured vibration mode shapes and longitudinal waveforms of the three helix angle ultrasonic augers.

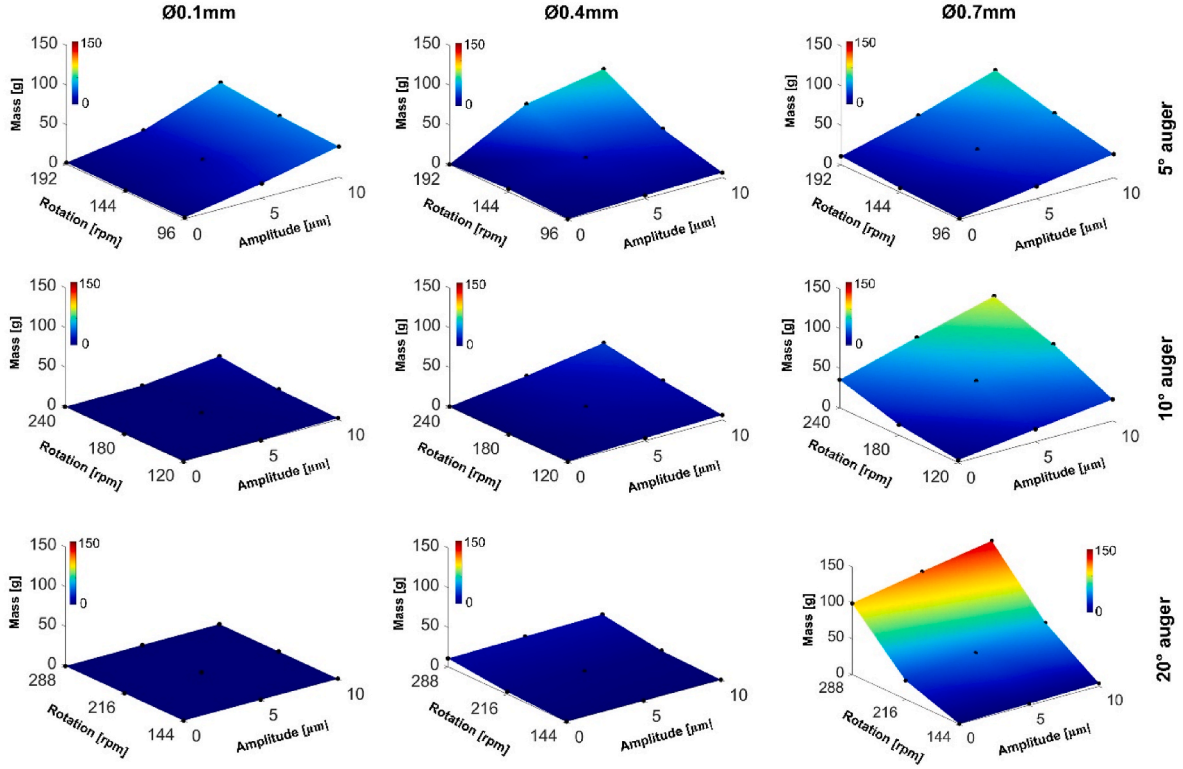

Fig. 6. Collected mass over 30 s, for three augers and three granular medium diameters, as a function of excitation amplitude and rotational speed. Each datapoint is the average of three experimental runs.

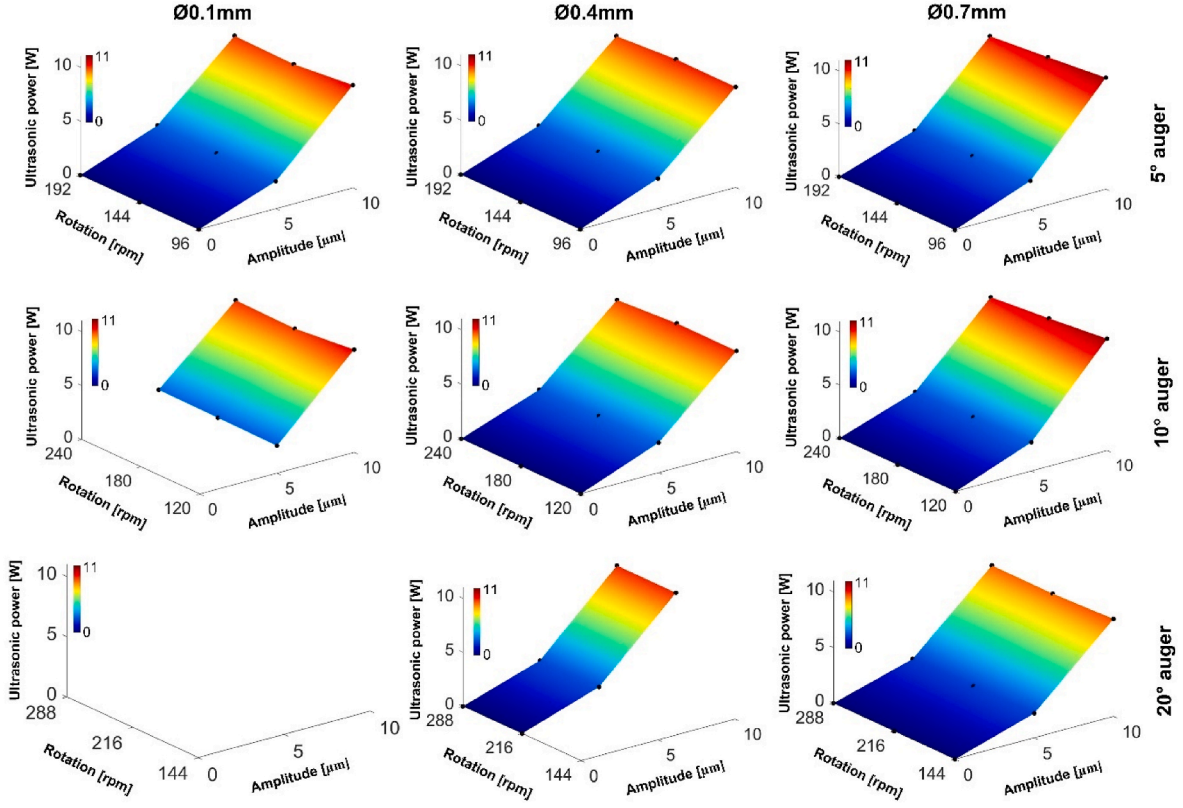

Fig. 7. Average ultrasonic power, for three augers and three granular medium diameters, as a function of excitation amplitude and rotational speed. Each datapoint is the average of three experimental runs. Omitted points reflect runs that did not succeed in lifting significant granular material.

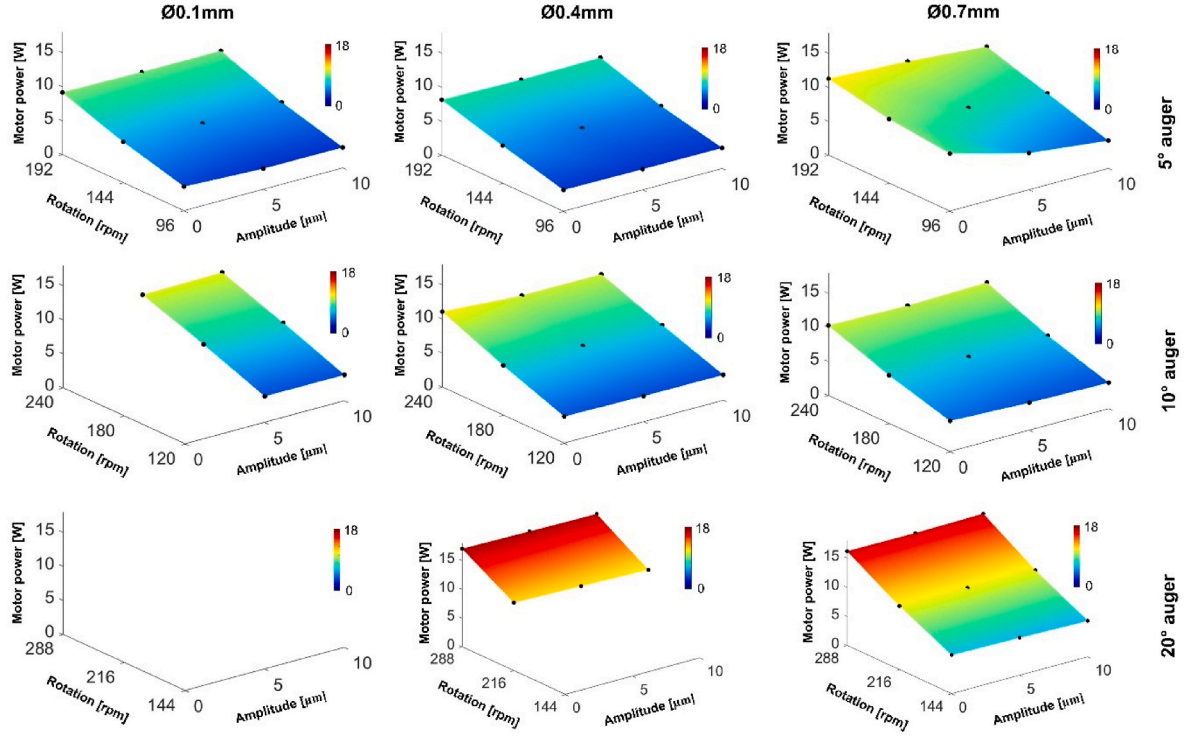

Fig. 8. Average motor power, for three augers and three granular medium diameters, as a function of excitation amplitude and rotational speed. Each datapoint is the average of three experimental runs. Omitted points reflect runs that did not succeed in lifting significant granular material.

extreme case of the 20° auger and the 0.1 mm material, no significant uplift was achieved at any speed or amplitude. In some cases, no significant uplift found nearby in the experimental parameter space either, particularly in the unsonicated and lower speed experiments. The 0.7 mm material appeared to be facilitated by ultrasonic excitation to the greatest degree, with sonication reducing the grinding noise heard in the

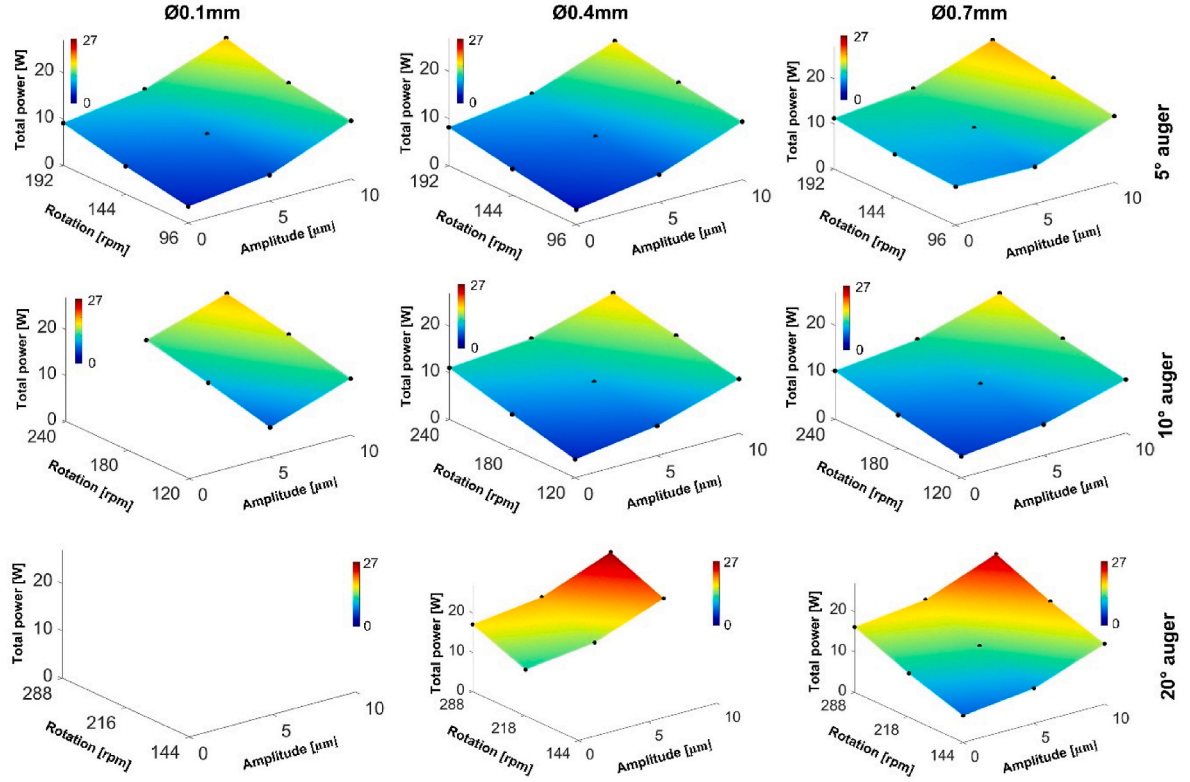

Fig. 9. Total power, for three augers and three granular medium diameters, as a function of excitation amplitude and rotational speed. Each datapoint is the average of three experimental runs. Omitted points reflect runs that did not succeed in lifting significant granular material.

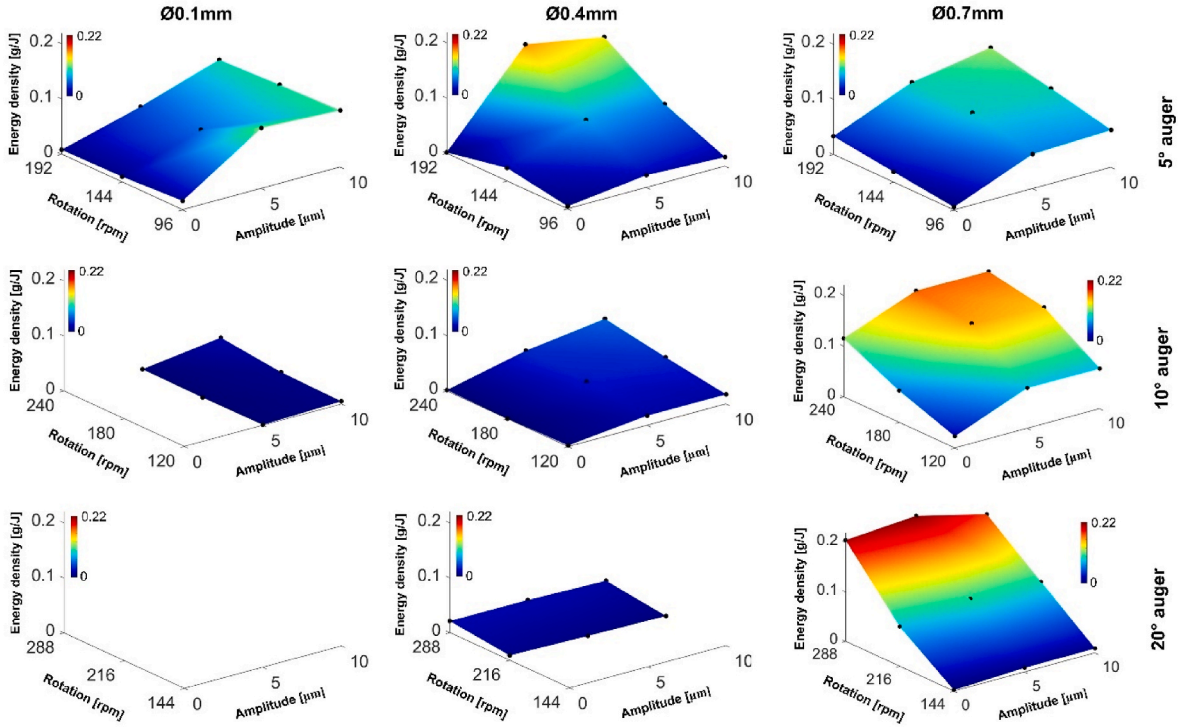

Fig. 10. Energy density, for three augers and three granular medium diameters, as a function of excitation amplitude and rotational speed. Each datapoint is the average of three experimental runs. Omitted points reflect runs that did not succeed in lifting significant granular material.

unsonicated cases and generally providing a more fluid-like appearance through the sides of the transparent tube. The grinding noise was likely generated by the larger individual particles becoming trapped between the auger and the tube, as this gap was nominally only 0.3 mm wider than the particles in question.

4.4. Ultrasonic power

The ultrasonic power required to maintain the chosen amplitude (Fig. 7) is, as expected, not a strong function of the auger selected, the rotational speed, or the granular material used – it simply rises with

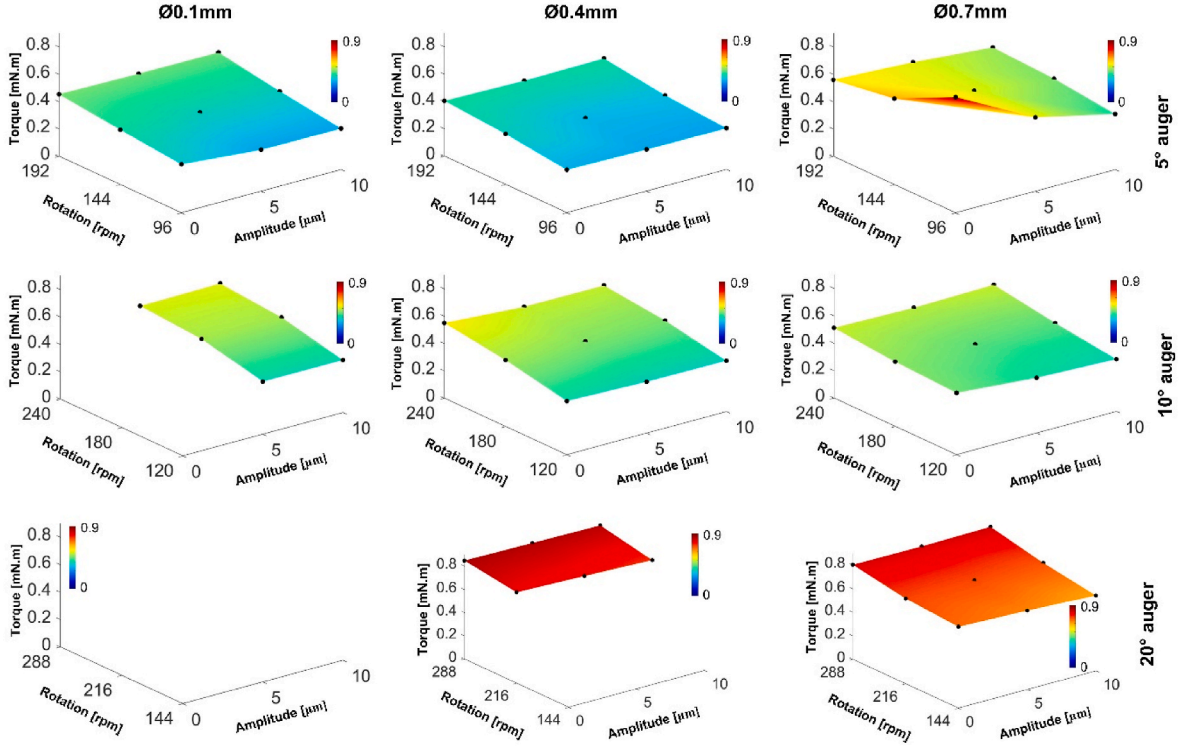

Fig. 11. Torque, for three augers and three granular medium diameters, as a function of excitation amplitude and rotational speed. Each datapoint is the average of three experimental runs. Omitted points reflect runs that did not succeed in lifting significant granular material.

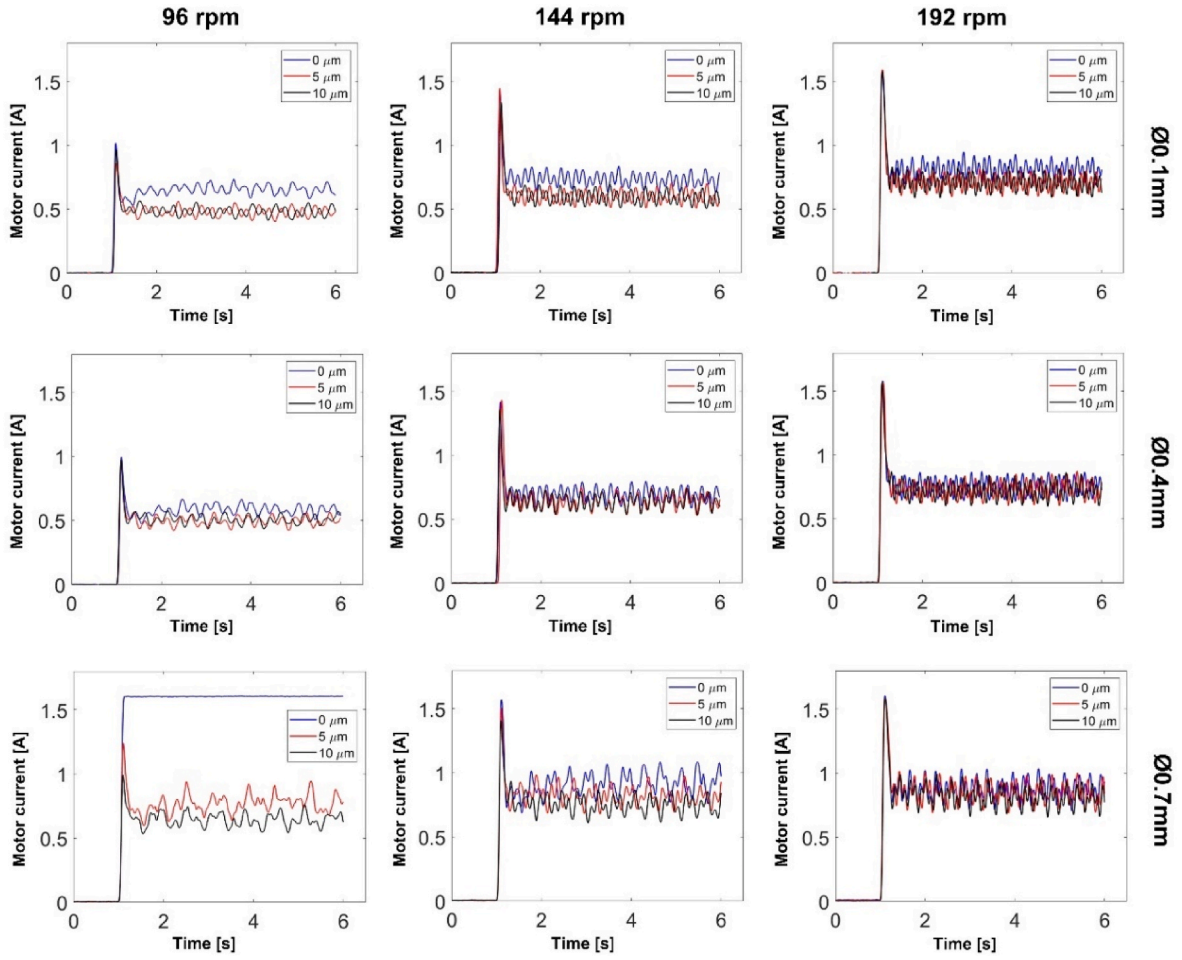

Fig. 12. Motor current as a function of ultrasonic transducer excitation amplitude and rotation for the 5° auger.

amplitude. In this figure, datapoints have been eliminated where the experiment did not result in significant throughput in Fig. 6.

4.5. Motor power

It was anticipated that ultrasonic vibration would reduce the rotational power requirement, and this effect is indeed observed in Fig. 8. It appears most strongly in the shallowest helix angles operating at the lowest speeds, in the coarsest materials: the 5° auger in the 0.7 mm material sees a reduction in motor power of 14%, 27%, and 52% for the 192 rpm, 144 rpm, and 96 rpm cases as displacement amplitude rises from 0 μm to 10 μm.

4.6. Total power

The total power consumption, calculated as the aggregation of the ultrasonic power and motor power for all three augers, is presented in Fig. 9. Unsurprisingly, the value increases with both the rotational speed and the displacement amplitude of the auger.

4.7. Energy density

To determine if the application of ultrasonics is energy-efficient, we must reflect that the greater mass flows seen in Fig. 6 must be balanced against the greater power requirements seen in Fig. 9. Dividing the results in one figure by the results in the other, and making minor scaling corrections, yields a new metric: grams per joule. This is shown in Fig. 10. This figure demonstrates that there is indeed a significant energy advantage in ultrasonically assisted augering, and it is again most consistently seen in the shallowest augers.

4.8. Motor torque

The final metric of interest is the motor torque. Using equation (2) and the motor power consumption values shown in Fig. 8, the torque exerted on each auger can be estimated. The results are presented in Fig. 11.

As expected, the steeper helix angle augers required larger torque. As was the case in the motor power analysis, the advantages of ultrasonic vibration are most strongly felt in the shallowest helix angles operating at the lowest speeds, in the coarsest materials. Under these circumstances, auger torque reductions on the order of 50% are possible.

4.9. Startup considerations

One particular aspect of augering systems is the startup torque, which is often higher than the steady-state torque [6]. By measuring the motor power as the auger is started under various levels of sonication, it should be possible to determine if this startup phenomenon is mitigated. The results are shown in Figs. 12–14 and they indicate, once again, that the strongest effects are seen in the shallowest augers, rotating at low speeds. Most significant are the results of the 5° auger, at 96 rpm, in the 0.7 mm material: in this case the unsonicated auger actually seized on startup, and drew the maximum 1.6 A of rated current without rotating for the duration of the experiment. The sonicated cases of the same experiment were able to start and continue to rotate throughout.

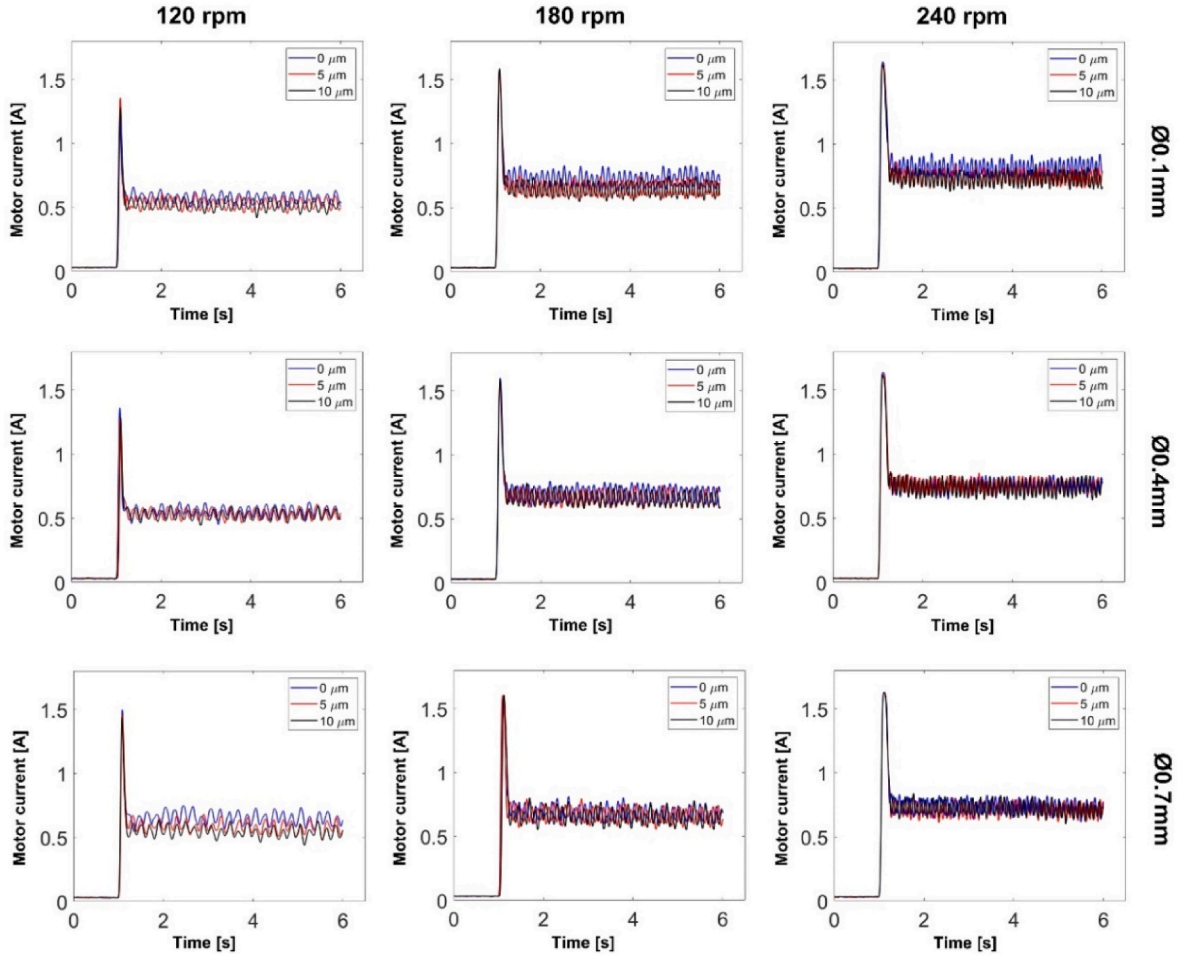

Fig. 13. Motor current as a function of ultrasonic transducer excitation amplitude and rotation for the 10° auger.

4.10. Repeatability

The 5° auger, at 96 rpm, in the 0.7 mm material, was consistently prone to seizure at startup, and so the effects of ultrasonics were examined in more details by cycling the vibration on and off. In this case, shown in Fig. 15, the motor initially stalled, but was able to start to move when the ultrasonics were cycled on. Multiple cycles have the consistent effect of reducing the motor current by around 50%, as was seen in Fig. 11.

5. Discussion

The effects observed in this study are believed to be associated with ultrasonically-enhanced fluidization in the space between the auger and the surrounding auger tube and, at least in part, a reduction in the effective drag forces therefore encountered at the auger surface itself.

Fluidization is a complex phenomenon and, of course, any granular material already satisfies some of the basic qualitative criteria for 'fluidity'. Granular materials will fill a container, but they can also maintain internal shear stresses, which is why they can cause an auger to seize. This is possible because stable chains of relatively few contacting particles can form dendritic patterns to transmit force into the far-field [7]. However, as is familiar in common materials such as mayonnaise, this apparent solidity can quickly give way to a viscous fluid-like behaviour at higher stress. The transition is more complex though, because in mayonnaise (a Bingham plastic) it occurs at a particular yield stress, but in granular media the breakdown (unjamming) is friction based [8], and influenced by pressure and particle shape [9]. It can also, apparently, be triggered by ultrasonic vibration [10].

If a granular material is fluidized, it will remain unjammed at all times. The grains lose their permanent contacts [11] and the load-bearing mechanism breaks down. Experiments have shown that bodies in fluidized granular media float according to their relative density, which suggests that the yield stress is reduced to zero [12] and that near-classical local viscosity can be recreated.

One method of characterizing the extent of this fluidization is granular temperature [13], a metric which rises as the velocity of individual grains increases with respect to the wider velocity field. Increasing granular temperature tends to reduce the apparent viscosity according to $\eta \sim T^{-0.5}$, where η is viscosity and T is granular temperature [14].

It appears possible that the ultrasonic vibration of the auger serves to increase the granular temperature and hence reduce viscosity near the auger itself, with the material having a reduced ability to transmit drag forces due to the breakdown mechanism described above. This would be somewhat analogous to the 'no-slip' condition in aerodynamic boundary layers and start to explain why augers with the longest flights (the shallow helix angles) can obtain the greatest relief. Naturally, the breakdown would be weaker at the unsonicated tube interface, and hence the increased friction differential would manifest as improved auger performance in terms of torque, speed, and throughput. Such an explanation would be consistent with the effects observed and described in this paper.

Another way to consider the same effect is to imagine that the sonicated rotating auger imparts less torque to the bulk material between the auger and the surrounding tube, which responds by rotating less

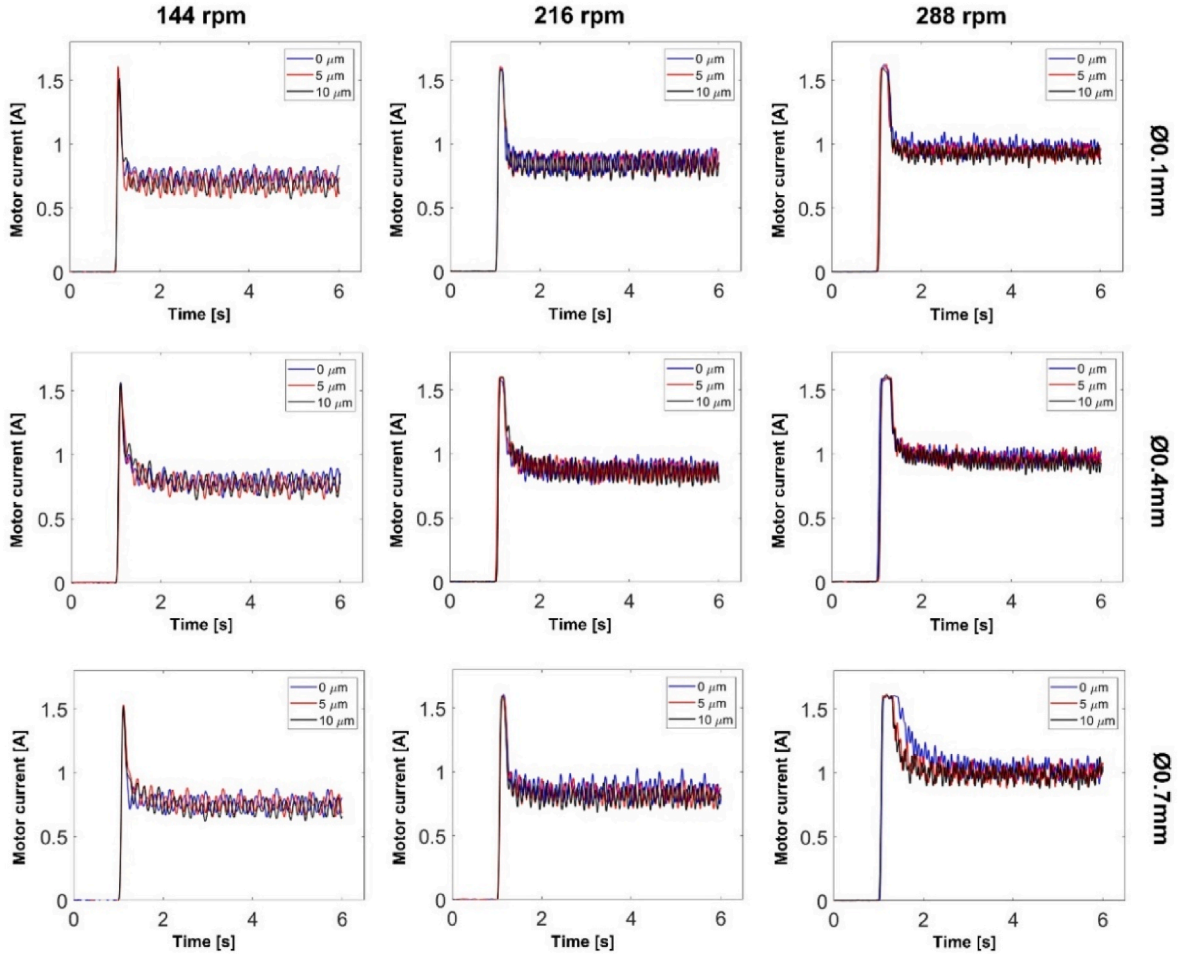

Fig. 14. Motor current as a function of ultrasonic transducer excitation amplitude and rotation for the 20° auger.

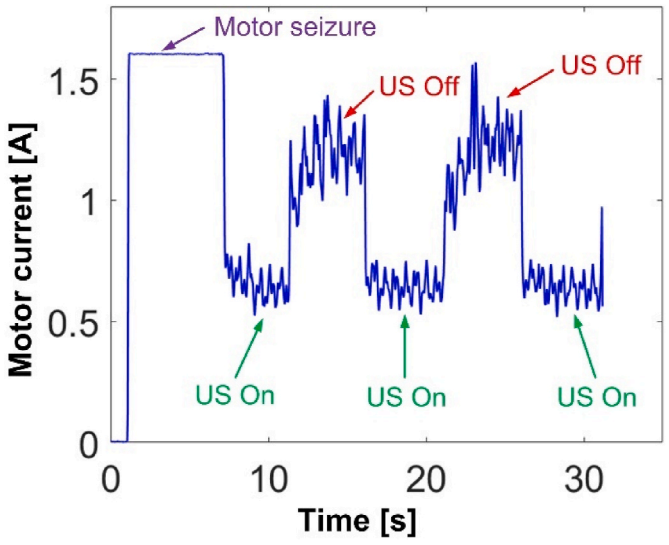

Fig. 15. Motor current monitoring when cycling ultrasonic vibration.

quickly against the walls of the tube itself. The relative speed of the flights with respect to the material would therefore be increased, and the auger would effectively operate at a higher speed than its true rpm would otherwise suggest.

That said the effects discussed above, in either explanation, may be expected to weaken somewhat at the nodes of vibration. Perhaps this is in fact the case, and the observations are simply an average across the whole auger, but they are no less interesting as a result.

The question also arises as to whether the separation between the auger and the surrounding tube is affected by sonication. In unsonicated augers this is an important parameter, because the system requires the influence of both surfaces to function: the (low friction) scroll must push the material upwards using the inclined plane effect, while the (high friction) tube must decelerate the material with respect to the auger core such that the scroll can move relative to the material and thus deploy its inclined plane effectively. Should the separation be too wide, the required constraint will not be felt and the auger will rotate without lifting. As an analysis of the consequences of the differential friction model indicates that steeper scroll angles require a higher rpm to operate [2], it is reasonable to expect that this failure mechanism should first manifest itself in steeper scroll angle devices. This is indeed what is seen in simulation [15].

The ideal separation is therefore small, but in practical terms it is a function of the particle size such that the material cannot easily fall past the scrolls. The results in this paper must be considered accordingly: the 0.7 mm particles generally performed best, perhaps because their size most closely approaches the 1 mm nominal gap between the auger and the tube. However, the extent to which the 'boundary layer' model might be applicable in a granular material only a few particles deep remains an open question.

Finally, on a practical note, the design of drilling systems requires that thought be applied to both the auger and the rock-breaking mechanism that creates the spoil in the first instance. The rock-

breaking mechanism can also be supported by ultrasonic excitation, and indeed rate-of-progress increases of up to 400% with respect to the unsonicated case have already been achieved in a range of rock types [16]. Therefore an ultrasonic drill tool that exploits both these effects in a single piece, as could easily be implemented, might well prove to be highly effective in shallow drilling.

6. Conclusion

The application of ultrasonic vibration to an auger has been shown to have a positive effect of the rate of material throughput, the torque requirements, and the overall energy efficiency of the system. This effect appears to be most significant when the helix angle is shallow and the auger is being rotated at the lower end of its operational speed band.

It is suspected that the mechanism is connected to a reduction in the effective friction coefficient of the auger scrolls against the granular material, which may in turn be connected to the fluidization effects of the ultrasonic vibration in the near-field.

The effect itself is consistent and repeatable, and it has particular applicability in shallow drill systems that require drillbits no longer than a few hundred mm, which could be engineered to resonate in a similar manner to the experimental rigs described herein. These implementations could easily be combined with an ultrasonically assisted drilling mechanism to create an integrated tool.

Declaration of competing interest

The authors declare that they have no known competing financial interests or personal relationships that could have appeared to influence the work reported in this paper.

Acknowledgment

This work was funded by the UK Space Agency, as the “Ultrasonically Assisted Augers” project.

Appendix A. Supplementary data

Supplementary data to this article can be found online at https://doi.org/10.1016/j.actaastro.2022.07.054.

References

[1] D. Firstbrook, K. Worrall, R. Timoney, F. Suñol, Y. Gao, P. Harkness, An Experimental Study of Ultrasonic Vibration and the Penetration of Granular Material, vol. 473, Proceeding of Royal Society A Mathematical, Physical and Engineering Sciences, 2017, p. 2198.
[2] K. Zacny, Methods for cuttings removal from holes drilled on Mars, Int. J. Mars Sci. Explor. 3 (2007) 42–56.
[3] A. Caronti, R. Carotenuto, M. Pappalardo, Electromechanical coupling factor of capacitive micromachined ultrasonic transducers, J. Acoust. Soc. Am. 113 (1) (2003) 279–288.
[4] P. Avitabile, Experimental Modal Analysis,” *Sound and Vibration Magazine* 35 (1) (2001) 1–15.
[5] V.I. Babitsky, A.N. Kalashnikov, F.V. Molodtsov, Autoresonant control of ultrasonically assisted cutting, Mechatronics 14 (1) (Feb. 2004) 91–114.
[6] M. Bortolamasi, J. Fottner, Design and Sizing of Screw Feeders, International Congress for Particle Technology, Nuremberg, Germany, 2001.
[7] J.F. Peters, M. Muthuswamy, J. Wibowo, A. Tordesillas, Characterization of force chains in granular material, Phys. Rev. E, Am. Phys. Soc. 72 (4) (2005) 1–8.
[8] O. Reynolds, On the dilatancy of media composed of rigid particles in contact, with experimental illustrations, Philos. Mag. J. Sci. Fifth Series 20 (127) (1885) 469–481.
[9] L. Staron, P.Y. Lagrée, P. Ray, S. Popinet, Scaling laws for the slumping of a Bingham plastic fluid, J. Rheol. 57 (4) (2013) 1265–1280.
[10] P. Lidon, N. Taberlet, S. Manneville, Grains unchained: local fluidization of a granular packing by focused ultrasound, Soft Matter 12 (2016) 2315–2324.
[11] I. Vardoulakis, Fluidisation in artesian flow conditions: hydromechanically stable granular media, Geotechnique 54 (2) (2004) 117–130.
[12] K. Nichol, M. Van Hecke, Flow-induced agitations create a granular fluid: effective viscosity and fluctuations, Phys. Rev. E, Am. Phys. Soc. 85 (6) (2012) 1–13.
[13] I. Goldhirsch, Introduction to granular temperature, Powder Technol. 182 (2) (2008) 130–136.
[14] A. Seguin, Y. Bertho, P. Gondret, J. Crassous, Dense granular flow around a penetrating object: experiment and hydrodynamic model, Phys. Rev. Lett., Am. Phys. Soc. 107 (4) (2011) 2–5.
[15] J. Hong, P. Talalay, M. Sysoev, X. Fan, DEM modeling of ice cuttings transportation by electromechanical auger core drills, Ann. Glaciol. 55 (68) (2017).
[16] X. Li, P. Harkness, Autonomous and ultrasonically assisted drilling in a range of rocks and ice, Ultrasonics 125 (2022), 106803.